Integrated Approach for Active Coupling of Structures and Fluids

Guru P. Guruswamy*
NASA Ames Research Center, Moffett Field, California

Strong coupling of structure and fluids is common in many engineering environments, particularly when the flow is nonlinear and very sensitive to structural motions. Such coupling can give rise to physically important phenomena, such as a dip in the transonic flutter boundary of a wing. The coupled phenomenon can be analyzed in closed form for simple cases that are defined by linear structural and fluid equations of motion. However, complex cases defined by nonlinear equations pose a more difficult task for solution. It is important to understand these nonlinear coupled problems, since they may lead to physically important new phenomena. Flow discontinuities, such as a shock wave, and structural discontinuities, such as a hinge line of a control surface of a wing, can magnify the coupled effects and give rise to new phenomena. To study such a strongly coupled phenomenon, an integrated approach is presented in this paper. The aerodynamic and structural equations of motion are simultaneously integrated by a time-accurate numerical scheme. The theoretical simulation is done using the time-accurate unsteady transonic aerodynamic equations coupled with modal structural equations of motion. As an example, the coupled effect of shock waves and hinge-line discontinuities are studied for aeroelastically flexible wings with active control surfaces. The simulation in this study is modeled in the time domain and can be extended to simulate accurately other systems where fluids and structures are strongly coupled.

Introduction

MANY physically important phenomena occur in engineering because of strong coupled interaction between structures and fluids. One such case is the use of wings with active control surfaces. Aerodynamic means can be developed through active controls to counter the forces and moments that drive flutter and dynamic instability. Use of active control is important for future aircraft, which will tend to be more flexible for high maneuverability.[1] So far, the theoretical aeroelastic studies with active control surfaces have been restricted to the linear subsonic and supersonic regimes.

Aeroelastic characteristics of wings are sensitive in the transonic regime because of flow nonlinearities and flow discontinuities from shock waves. The rapid changes in the aerodynamic forces in the transonic regime can give rise to nonclassical phenomena such as a "transonic dip."[2] The combined effect of the shock wave and the flow discontinuity due to the presence of the hinge line of the control surface can have a pronounced influence on both aerodynamic and aeroelastic performances of wings. This pronounced influence of the control surface movement on the wing aerodynamics in the transonic regime can be used constructively to prevent aeroelastic oscillations. Such use of control surfaces is becoming popular through the development of active control technology. However, one should carefully watch for any nonclassical aeroelastic phenomenon that is common in transonic flows. For this, structures, aerodynamics, and active control equations should be simultaneously solved.

In order to study the coupling of complex physical systems like nonlinear flows and wing structures, it is important to use well-understood equations and solution procedures. Therefore, the familiar modal form of structural equations of motion is used in this analysis. The modal data needed for structure is accurately obtained by the well-developed finite-element analysis. For fluids, the well-defined transonic small perturbation (TSP) flow equations of motion are used. The aerodynamic equations are solved by the robust time-accurate alternating-direction implicit finite-difference method. The reasons for employing the TSP flow equations are as follows.

The lack of efficient computational tools had previously restricted the theoretical simulations of the coupling of structures and fluids to the linear subsonic and supersonic regimes. Developments in computational fluid dynamics have made available efficient methods for computing the unsteady transonic aerodynamic loads. To date, the most advanced computational methods for aeroelastic applications are those based on the transonic potential flow theory. The unsteady equations of motion based on the transonic small perturbation (TSP) theory have been accurately solved by using finite-difference schemes based on the alternating-direction implicit method for two-[3] and three-dimensional flows.[4] The TSP equation has been coupled successfully with the structural equations of motion of typical sections[5] and wings.[4] Several applications have shown that practical aeroelastic responses can be obtained by using the TSP theory coupled with modal equations of motion.[6]

In this work, a procedure for simulating the active coupling of structures and nonlinear flows is presented. The approach is oriented toward synthesizing active controls of aeroelastically oscillating wings with unsteady transonics in the time domain. Using this procedure, the complex role of shock waves on active controls is studied. The scheme presented in this work is general in nature and can be extended to study engineering problems where structures and fluids are strongly coupled through some type of active control system.

Unsteady Transonic Flow Equations

The modified three-dimensional small-disturbance unsteady transonic equation of motion is given by

$$A\phi_{tt} + B\phi_{xt} = [E\phi_x + F\phi_x^2 + G\phi_y^2]_x + [\phi_y + H\phi_x\phi_y]_y + [\phi_z]_z \quad (1)$$

Received June 3, 1987; revision received April 20, 1988.

*Research Scientist. Associate Fellow AIAA.

where $A = M_\infty^2$, $B = 2M_\infty^2$, $E = (1 - M_\infty^2)$, $F = -(\frac{1}{2})(\gamma + 1)M_\infty^2$, $G = -(\frac{1}{2})(\gamma - 3)M_\infty^2$, $H = -(\gamma - 1)M_\infty^2$, ϕ is the disturbance velocity potential, M_∞ is the freestream Mach number, and γ is the ratio of specific heats. This equation is solved by using an efficient time-accurate finite-difference scheme based on the alternating-direction implicit scheme. Details are given in Refs. 4 and 7.

The thin-wing surface-flow tangency condition that is satisfied at any point on the mean chord plane is given by

$$\phi_z = f_x - \alpha_0 - \alpha(t) \text{ for } 0.0 < x < x_{\text{hinge}} \tag{2a}$$

$$\phi_z = f_x - \alpha_0 - \alpha(t) - \delta(t) \text{ for } x_{\text{hinge}} < x < 1.0 \tag{2b}$$

where $f(x)$ denotes the airfoil surface function, α_0 is the local mean angle of attack, $\alpha(t)$ is the local angle of attack due to flexibility of the wing, δ is the angular deflection of the control surface, and x is the distance from the leading edge in local chord length. The changes in the boundary condition on the wing surface caused by control-surface oscillations are modeled using Eqs. (2).

Active Control Surfaces

In this work, it is assumed that a control law is known from detailed control theory analysis for a given configuration. Using the present procedure, the coupled phenomenon of structures, aerodynamics, and active controls can be accurately simulated. A typical control law in the time domain can be assumed as

$$\delta = G_1 h_1(t) e^{i\psi_1} + G_2 \alpha_1(t) e^{i\psi_2} \tag{3}$$

where δ is the control-surface deflection, G_1 and G_2 are gain factors, h_1 is the deflection at a selected point on the wing, α_1 is the angle of attack at a selected span station, and ψ_1 and ψ_2 are phase angles. By representing the active control law in the preceding form, the coupled phenomenon of structures, aerodynamics, and active controls can be studied in realistic time domain.

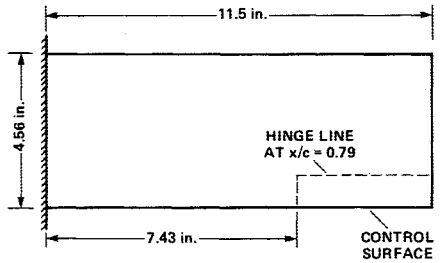

Fig. 1 Rectangular wing planform with part-span trailing-edge flap.

Aeroelastic Equations of Motion

The governing aeroelastic equations of motion of a flexible wing are obtained by using the Rayleigh-Ritz method (Ref. 8, Chap. 3). In this method, the resulting aeroelastic displacements at any time are expressed as a function of a finite set of selected modes. The contribution of each selected mode to the total motion is derived by Lagrange's equation. Furthermore, it is assumed that the deformation of the continuous wing structure can be represented by deflections at a set of discrete points. This assumption facilitates the use of discrete structural data, such as the modal vector, the modal stiffness matrix, and the modal mass matrix. In this study, the finite-element method is employed to obtain the modal data. Both the stiffness and the mass of the control surface are included in the analysis.

It is assumed that the deformed shape of the wing can be represented by a set of discrete displacements at selected nodes. From the modal analysis, the displacement vector $\{d\}$ can be expressed as

$$\{d\} = [\phi]\{q\} \tag{4}$$

where $[\phi]$ is the matrix of displacements of the natural vibration modes interpolated to the finite-difference grid points used to model the flow and $\{q\}$ is the generalized displacement vector.

The final matrix form of the aeroelastic equations of motion is

$$[M]\{\ddot{q}\} + [G]\{\dot{q}\} + [K]\{q\} = \{F\} \tag{5}$$

where $[M]$, $[G]$, and $[K]$ are modal mass, damping, and stiffness matrices, respectively; $\{F\}$ is the aerodynamic force vector defined as $(\frac{1}{2})\rho U_\infty^2[\phi]^T[A]\{\Delta C_p\}$, and $[A]$ is the diagonal area matrix of the aerodynamic control points, which are the same as the grid points used for the finite-difference modeling of the flow.

These equations of motion are solved by numerically integrating Eq. (5) in time by the linear acceleration method. As-

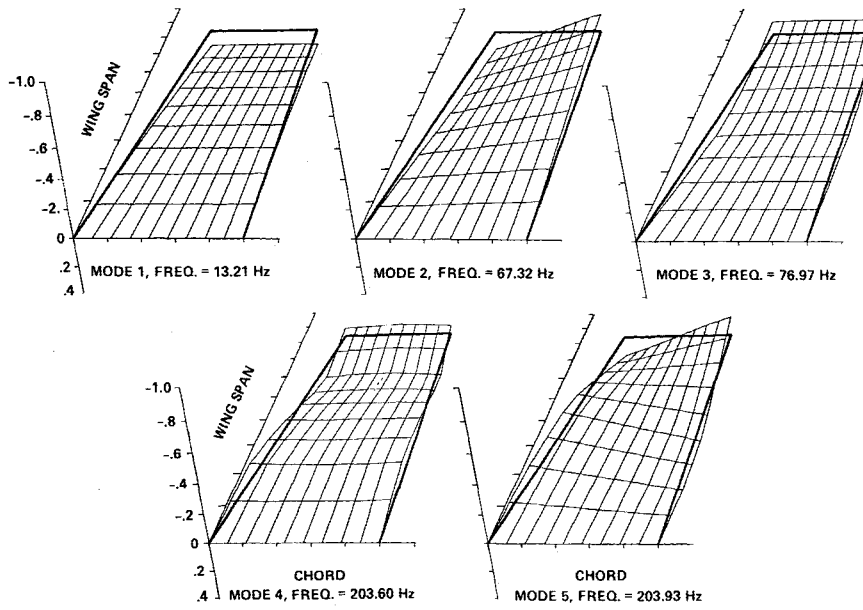

Fig. 2 Mode shapes of the rectangular wing.

suming a linear variation of the acceleration, the velocities and displacements at the end of a time interval t can be derived as follows:

$$\{\dot{q}\}_t = \{\dot{q}\}_{t-\Delta t} + (\Delta t/2)\{\ddot{q}\}_{t-\Delta t} + (\Delta t/2)\{\ddot{q}\}_t \tag{6a}$$

$$\{q\}_t = \{q\}_{t-\Delta t} + (\Delta t)\{\ddot{q}\}_{t-\Delta t} + (\Delta t^2/3)\{\ddot{q}\}_{t-\Delta t} + (\Delta t^2/6)\{\ddot{q}\}_t \tag{6b}$$

$$\{\ddot{q}\}_t = [D](\{F\}_t - [G]\{v\} - [K]\{w\}) \tag{6c}$$

where

$$[D] = [[M] + (\Delta t/2)[G] + (\Delta t^2/6)\{K\}]^{-1}$$

$$v = \{\dot{q}\}_{t-\Delta t} + (\Delta t/2)\{\ddot{q}\}_{t-\Delta t}$$

$$w = \{q\}_{t-\Delta t} + (\Delta t)\{\dot{q}\}_{t-\Delta t} + (\Delta t^2/3)\{\ddot{q}\}_{t-\Delta t}$$

These equations also can be derived by using the second-order-accurate central-difference scheme. Since the preceding equations are explicit in time, its time-step size is restricted by stability. However, the time-step size required to solve time-accurately the aerodynamic Eq. (1) is always far less than the time-step size required to obtain stable and accurate solution using the given numerical integration scheme.[5] To obtain physically meaningful time-accurate solutions, it is necessary to use the same time-step size in integrating Eq. (1) and Eq. (5). Also, the preceding scheme is numerically nondissipative and does not lead to any nonphysical aeroelastic phenomenon.

The step-by-step integration procedure for obtaining the aeroelastic response was performed as follows. Assuming that freestream conditions and wing-surface boundary conditions were obtained from a set of selected starting values of the generalized displacement, velocity, and acceleration vectors, the generalized aerodynamic force vector $\mathbf{F}(t)$ at time t was computed by solving Eq. (1). Using this aerodynamic vector, the generalized displacement, velocity, and acceleration vectors for the time level t are calculated by Eq. (5). From the generalized coordinates computed at the time level t, the new boundary conditions on the surface of the wing are computed. At the same time, the control-surface angle of attack $\delta(t)$ is computed using the active control law given by Eq. (3). With these new boundary conditions, the aerodynamic vector $\{F(t)\}$ at the next time level $t + \Delta t$ is computed by using Eq. (1). This process is repeated every time step to solve the aerodynamic and structural equations of motion forward in time until the required response is obtained. It is noted that the alternate-direction implicit scheme used to solve the flow equation [Eq. (1)] requires the boundary conditions both at time level t and $t + \Delta t$. These required boundary conditions are computed by solving the aeroelastic equations of motion [Eq. (5)] both at time t and $t + \Delta t$.

Coupling of Control and Aeroelastic Equations

The control surface is modeled within the limitations of the transonic small-perturbation theory. The interaction between the control surface and the flow is accomplished through the wing boundary conditions given by Eq. (2). At every time step, the aeroelastic equation of motion [Eq. (4)] is solved for new values of the generalized displacement vector $\{q\}$. Using this vector, the vector of angles of attack $\{\alpha(t)\}$ required in Eq. (2) are computed by

$$\{\alpha(t)\} = [\phi']\{q(t)\} + (1/U_\infty)[\phi]\{\dot{q}(t)\} \tag{7}$$

where $[\phi']$ denotes the matrix of streamwise slopes of the natural vibration modes interpolated to the aerodynamic grid points.

When the control surface is active, the deflection angle is computed using Eq. (3). The value of the feedback displacement $h_1(t)$ at a selected grid point is taken from the displacement vector $\{d\}$ computed by Eq. (5), and the value of the feedback angle of attack $\alpha_1(t)$ at a selected point is taken from the angular displacement vector $\{\alpha(t)\}$ computed by Eq. (7). With the modified boundary conditions, the new values of aerodynamic forces are computed. This procedure is repeated for every time step.

Numerical Illustration

In order to illustrate the practical application of the scheme developed, an aeroelastic case of a typical uniform rectangular wing of aspect ratio 5.0 with a trailing-edge control surface, shown in Fig. 1, was selected. The mode shapes and frequencies required for the modal equations of motion [Eq. (5)] were accurately computed by a 16-degree-of-freedom rectangular finite element.[9] Figure 2 shows the mode shapes and frequencies of the first five natural modes for the wing. Using this modal data, the aeroelastic equation of motion [Eq. (5)] was solved by the time integration method described earlier.

Aeroelastic analyses were conducted for six Mach numbers from 0.715 to 0.905, with and without the active control surface. All responses were started with modally displaced initial conditions obtained by giving unit values to the first two generalized coordinates. To begin with, the aeroelastic equations were integrated without the active control surface. At a selected time, the control surface was made active and the integration process was continued.

Mach numbers selected represent flow conditions ranging from subsonic, to transonic with weak shock, to transonic with strong shock. The active control law selected corresponds to $G_1 = 0.0$, $G_2 = 0.5$, $\psi_1 = 0.0$, and $\psi_2 = 0.0$ of Eq. (3). The feedback values of the displacement $h_1(t)$ and the angle of attack $\alpha_1(t)$ were taken from the midpoint of the wing tip. The control law parameters were selected such that with a positive (trailing-edge-down) tip angle of attack, the flap angle would be positive to counter the tip angle.

In Figs. 3–6, the first, second, and third modal responses are shown with and without active control for Mach numbers

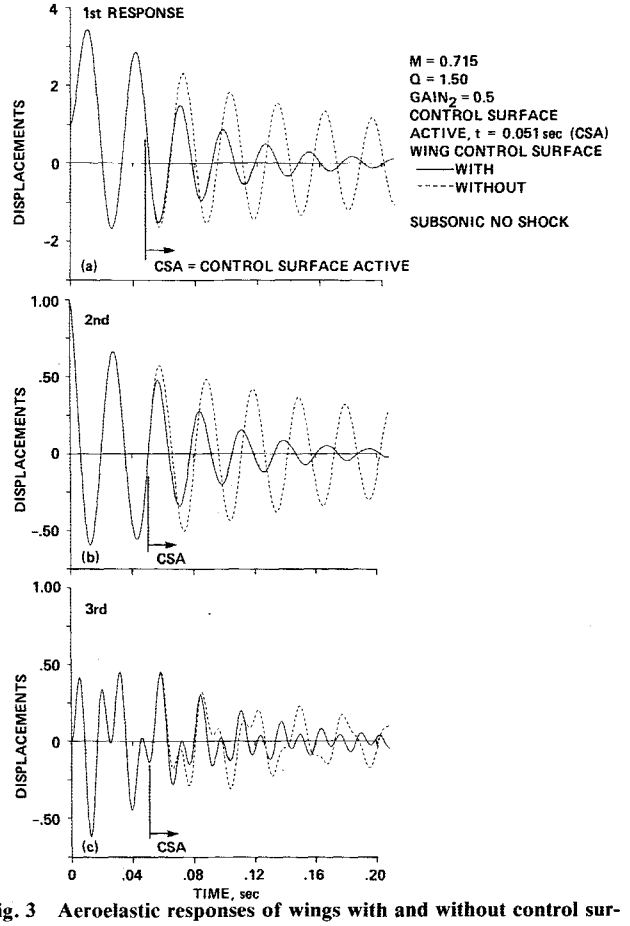

Fig. 3 Aeroelastic responses of wings with and without control surfaces at $M = 0.715$.

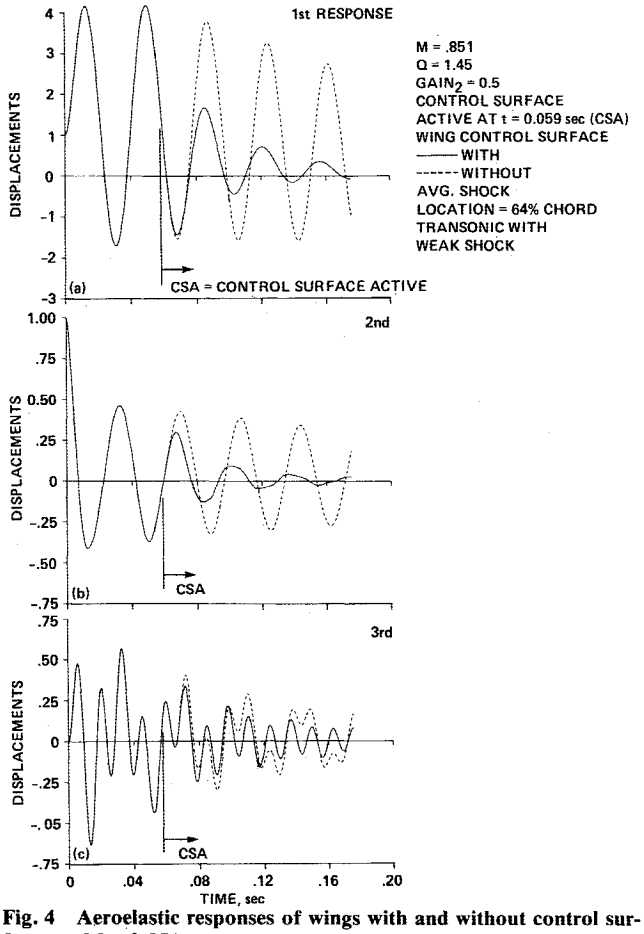

Fig. 4 Aeroelastic responses of wings with and without control surfaces at $M = 0.851$.

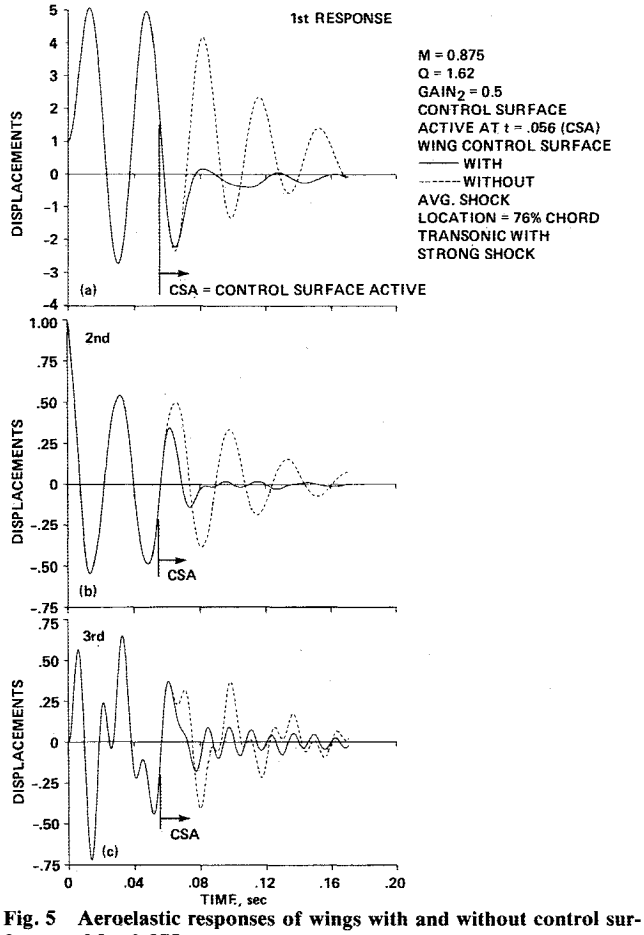

Fig. 5 Aeroelastic responses of wings with and without control surfaces at $M = 0.875$.

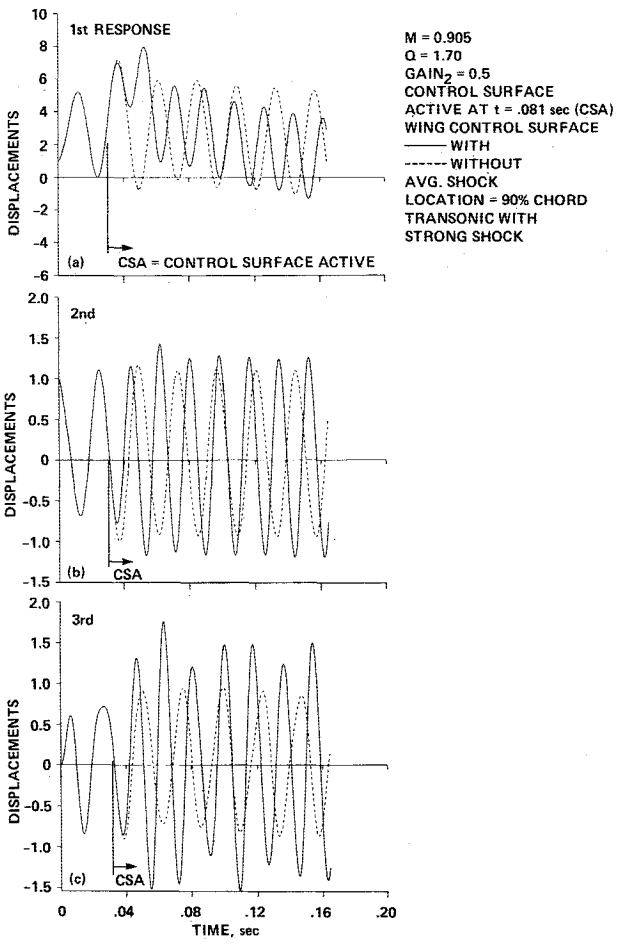

Fig. 6 Aeroelastic responses of wings with and without control surfaces at $M = 0.905$.

0.715, 0.851, 0.875, and 0.905, respectively. At the subsonic Mach number of 0.715, the selected control law is effective, as seen in Fig. 3. The effectiveness of the same control law increases as the flow becomes transonic. By observing the rate of dampings in Figs. 4 and 5, it can be concluded that the control law is more effective at the transonic Mach number and when the shock wave is in front of the hinge line. This increase in effectiveness is a direct result of the increase in the rate of change in aerodynamic forces due to control-surface deflections. However, as seen in Fig. 6 for $M = 0.905$, when the shock wave is aft of the control surface hinge line, it appears that the control surface is ineffective. The possible reason for this phenomenon can be further explained by studying the responses of the first generalized displacement in detail.

The effect of Mach number and the mean location of the shock wave on aeroelastic responses of the first generalized displacement is summarized in Fig. 7. Based on these responses, the effectiveness of the active control law is computed. The effectiveness of the active control law is defined as the ratio of the damping coefficients with active control to those without active control. In this analysis, the damping coefficient is defined as the ratio of the maximum displacement of the fourth cycle to the maximum displacement of the fifth cycle. Figure 8 shows the plots of the control-surface effectiveness and the corresponding shock-wave location with respect to Mach number. As seen in Fig. 8, the effectiveness of the active control increases with the increase in Mach number until about $M = 0.88$. After $M = 0.88$, the effectiveness of the active control rapidly decreases with the increase in Mach number. It can be noted in Fig. 8 that at about $M = 0.88$, the mean location of the shock wave crosses the hinge line. The fact that the control surface becomes ineffective when the shock wave crosses the hinge line leads to the conclusion that the combined influence of the discontinuities from the shock

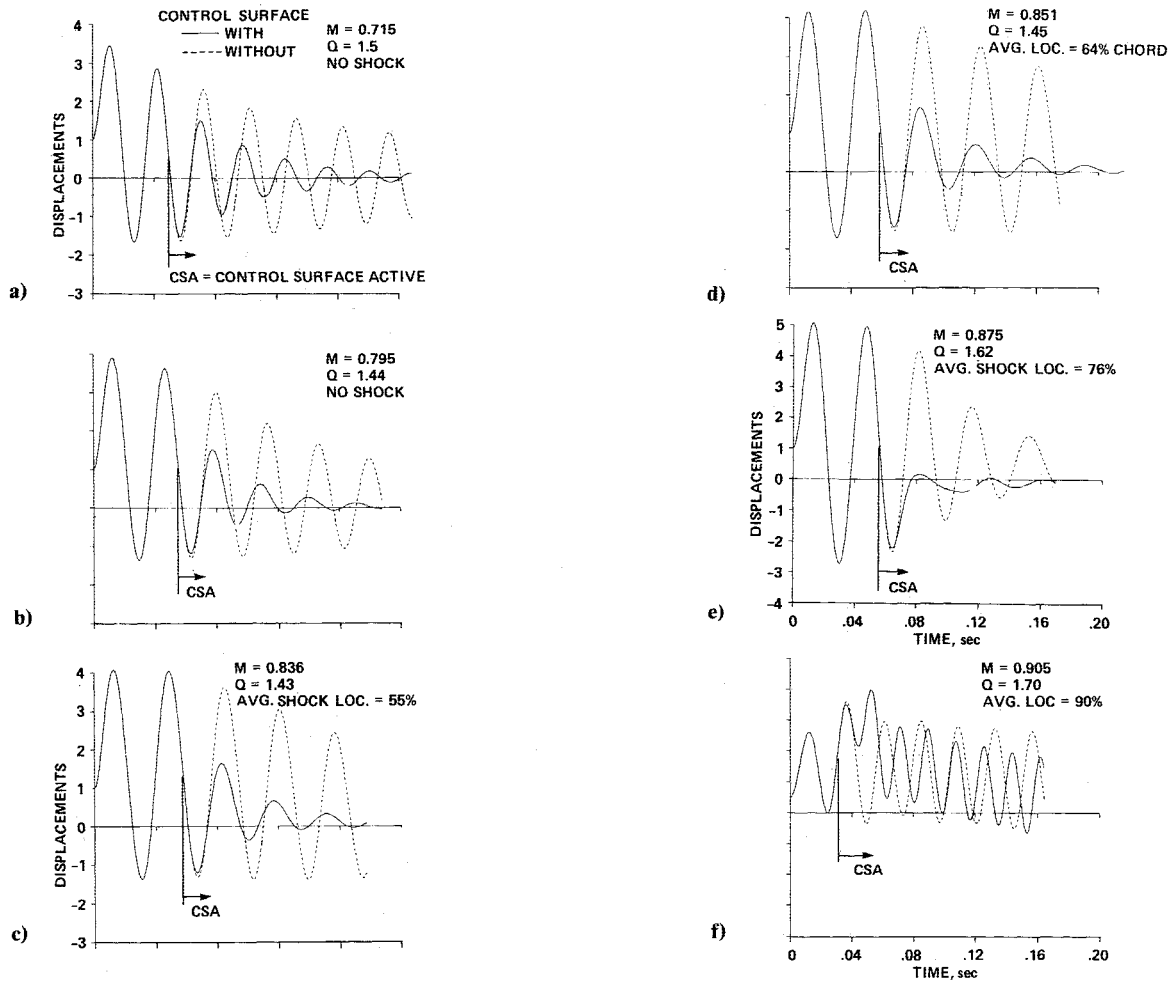

Fig. 7 Summary of aeroelastic responses of the first mode with and without control surfaces for six Mach numbers.

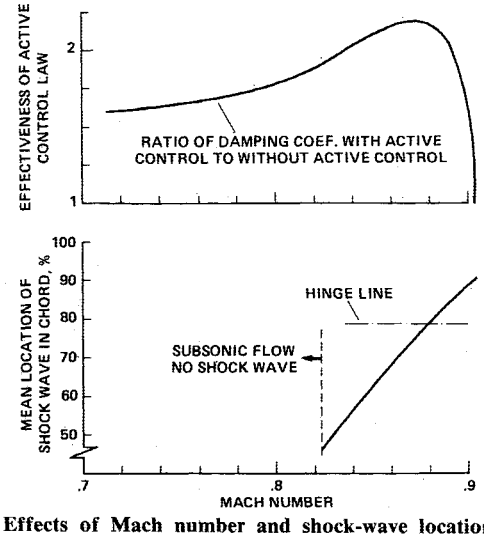

Fig. 8 Effects of Mach number and shock-wave location on the effectiveness of the active control surface.

wave and hinge line block the flow of aerodynamic information between the zones separated by the hinge line.

An additional explanation for the rapid drop in the effectiveness of the active control for Mach numbers greater than 0.88 can be given from the observation that the flow is predominantly supersonic in front of the hinge line. The aerodynamic forces on the wing are less sensitive to control-surface oscillations when flow becomes more supersonic. This fact has been observed in both wind-tunnel experiments[10] and computations.[11] From these observations, it may be concluded that the presence of the shock wave and its location is important and needs to be accounted for in designing of an effective control law.

The preceding numerical illustration shows that the integrated analysis scheme presented in this paper can be employed to efficiently simulate physical phenomenon where fluids and structures are actively coupled. This scheme has been successfully incorporated[11] in XTRAN3S-Ames, the NASA-Ames version of the Air Force/NASA XTRAN3S,[12] a general-purpose software that is being developed to simulate time accurately the aeroelastic phenomena of aircraft in the transonic regime. The scheme presented in this work can also be used to simulate the active coupled interaction of fluids and structures in other engineering environments.

Conclusions

A numerical scheme has been presented to simulate the phenomenon where structures and aerodynamics are actively coupled. The nonlinear aerodynamic equations are solved by the appropriate finite-difference method, and the structural equations are solved by the finite-element method. A time-domain active relation between structures and aerodynamics is used. Fluids, structures, and active controls are integrated time accurately by an efficient numerical scheme. The scheme has been illustrated for the coupling of the complex nonlinear transonic flows with wing-structural responses through an active control surface. Computations for a rectangular wing show that the present procedure efficiently works for actively coupling flexible structures with complex unsteady transonics. For this case, the important role of the shock wave and its location on the coupled response is illustrated. It is also shown that control laws that do not account for strong coupled phenomena of fluids and structures may not be effective in the transonic regime. Since the present study is in the time domain, it can be

implemented easily for realistic numerical simulation of active and strong coupling of fluids and structures.

Acknowledgments

This work was supported by NASA Ames and Wright Patterson Air Force Base. The author is grateful to Mr. Eugene L. Tu and Dr. Peter M. Goorjian of NASA Ames and Mr. Larry J. Huttsell of Wright Patterson Air Force Base for their many helpful suggestions made during the course of this study.

References

[1]Noll, T. E. and Huttsel, L. J., "Wing Store Active Flutter Suppression—Correlation of Analyses and Wind-Tunnel Data," *Journal of Aircraft,* Vol. 16, July 1979, pp. 491–497.

[2]Ashley, H., "Role of Shocks in the 'Sub-Transonic' Flutter Phenomenon," *Journal of Aircraft,* Vol. 17, March 1980, pp. 187–197.

[3]Ballhaus, W. F. and Goorjian, P. M., "Implicit Finite Difference Computations of Unsteady Transonic Flows About Airfoils," *AIAA Journal,* Vol. 15, Dec. 1977, pp. 1728–1735.

[4]Borland, C. J. and Rizzetta, D. P., "Nonlinear Transonic Flutter Analysis About Airfoils," *AIAA Journal,* Vol. 20, Nov. 1982, pp. 1606–1615.

[5]Guruswamy, G. P. and Yang, T. Y., "Aeroelastic Time Response Analysis of Thin Airfoils by Transonic Code LTRAN2." *Computers and Fluids,* Vol. 9, No. 4, Dec. 1980, pp. 409–425.

[6]Guruswamy, G. P., Goorjian, P. M. Ide, H., and Miller, G. D., "Transonic Aeroelastic Analysis of the B-1 Wing," *Journal of Aircraft,* Vol. 23, July 1986, pp. 547–553.

[7]Guruswamy, G. P. and Goorjian, P. M., "Efficient Algorithm for Unsteady Transonic Aerodynamics of Low-Aspect Ratio Wings," *Journal of Aircraft,* Vol 22, March 1985, pp. 193–199.

[8]Bisplinghoff, R. L., Ashley, H., and Halfman, R. L., *Aeroelasticity,* Addison-Wesley, Reading, MA, Nov. 1957.

[9]Guruswamy, P. G., "Special-Purpose Finite Element Programs, " *Finite Element Structural Analysis,* edited by Yang T. Y. Prentice-Hall, Englewood Cliffs, NJ, 1986, Chap. 13.

[10]Persoon, A. J., Roos, R., and Schippers, P., "Transonic and Low Supersonic Wind Tunnel Tests on a Wing with Inboard Control Surface," Air Force Flight Dynamics Lab., Wright-Patterson AFB, OH, AFFDL-TR-80-3146, Dec. 1980.

[11]Guruswamy, G. P., Tu, E. L., and Goorjian, P. M., "Transonic Aeroelasticity of Wings with Active Control Surfaces," AIAA Paper 87-0709-CP, April 1987.

[12]Borland, C. J. and Rizzetta, D. P., "Transonic Unsteady Aerodynamics for Aeroelastic Applications: Vol. I—Technical Development Summary," Wright Aeronautical Lab., Wright-Patterson AFB, OH, AFWAL-TR-80-3107, June 1982.

This article has been cited by:

1. Ronald N. Kostoff, Russell M. Cummings. 2013. Highly cited literature of high-speed compressible flow research. *Aerospace Science and Technology* **26**:1, 216-234. [CrossRef]
2. Terry L. Holst. 2009. Transonic flow potential method development at Ames research center. *Computers & Fluids* **38**:3, 482-490. [CrossRef]
3. 2008. Flow Analysis of Magnetic Fluid in Inlet Length Region between Parallel Plates. *Journal of Fluid Machinery* **11**:2, 7-12. [CrossRef]
4. 2008. *Journal of Fluid Machinery* **11**:2, 71-76. [CrossRef]
5. Mark J. Wilson, Mehmet Imregun, Abdulnaser I. Sayma. 2007. The Effect of Stagger Variability in Gas Turbine Fan Assemblies. *Journal of Turbomachinery* **129**:2, 404. [CrossRef]
6. L. Djayapertapa, C.B. Allen. 2004. Simulation of transonic flutter and active shockwave control. *International Journal of Numerical Methods for Heat & Fluid Flow* **14**:4, 413-443. [CrossRef]
7. Volker Carstens, Ralf Kemme, Stefan Schmitt. 2003. Coupled simulation of flow-structure interaction in turbomachinery. *Aerospace Science and Technology* **7**:4, 298-306. [CrossRef]
8. Volker Carstens, Joachim Belz. 2001. Numerical Investigation of Nonlinear Fluid-Structure Interaction in Vibrating Compressor Blades. *Journal of Turbomachinery* **123**:2, 402. [CrossRef]
9. Damien M. Guillot, Peretz P. Friedmann. 2000. Fundamental Aeroservoelastic Study Combining Unsteady Computational Fluid Mechanics with Adaptive Control. *Journal of Guidance, Control, and Dynamics* **23**:6, 1117-1126. [Citation] [PDF] [PDF Plus]
10. Terry L. Holst. 2000. Transonic flow computations using nonlinear potential methods. *Progress in Aerospace Sciences* **36**:1, 1-61. [CrossRef]
11. Serge Piperno. 1997. Explicit/implicit fluid/structure staggered procedures with a structural predictor and fluid subcycling for 2D inviscid aeroelastic simulations. *International Journal for Numerical Methods in Fluids* **25**:10, 1207-1226. [CrossRef]
12. P. P. Friedmann, D. Guillot, E. Presente. 1997. Adaptive Control of Aeroelastic Instabilities in Transonic Flow and Its Scaling. *Journal of Guidance, Control, and Dynamics* **20**:6, 1190-1199. [Citation] [PDF] [PDF Plus]
13. P. Friedmann, D. Guillot, E. Presente, P. Friedmann, D. Guillot, E. PresenteAdaptive control of aeroelastic instabilities in transonic flow and its scaling . [Citation] [PDF] [PDF Plus]
14. G. A. Gerolymos, I. Vallet, A. Bolcs, P. Ott. 1996. Computation of unsteady three-dimensional transonic nozzle flows using k-epsilon turbulence closure. *AIAA Journal* **34**:7, 1331-1340. [Citation] [PDF] [PDF Plus]
15. M. Rais-Rohani, R.T. Haftka, B. Grossman, E.R. Unger. 1992. Integrated aerodynamic-structural-control wing design. *Computing Systems in Engineering* **3**:6, 639-650. [CrossRef]
16. G.P. Guruswamy. 1990. Ensaero—A multidisciplinary program for fluid/structural interaction studies of aerospace vehicles. *Computing Systems in Engineering* **1**:2-4, 237-256. [CrossRef]